Journal of Materials Science and Chemical Engineering, 2025, 13(10), 62-84
https://www.scirp.org/journal/msce
ISSN Online: 2327-6053
ISSN Print: 2327-6045

Synthesis of a Modified Biosorbent from Lignocellulosic Biomass: Comparative Adsorption Performance with an Activated Carbon of the Same Origin

Faouzou Ouro-Agoro[1,2,3*], Ibrahim Tchakala[1], Koffi Fiaty[3], Catherine Charcosset[3], Laurent Vanoye[4], Akpénè Amenuvevega Dougna[2], Seyf-Laye Alfa-Sika Mande[1,2], Limam Moctar Bawa[1]

[1]Laboratoire d'Hydrologie Appliquée et Environnement, LHAE, Faculté Des Sciences, Université de Lomé, Lomé, Togo
[2]Laboratoire de Chimie Organique et Science de l'Environnement, LaCOSE, Faculté Des Sciences et Techniques, Université de Kara, Kara, Togo
[3]Université Claude Bernard Lyon-1, Laboratoire d'Automatique, de Génie des Procédés et de Génie Pharmaceutique (LAGEPP), Bât CPE-Lyon, UMR CNRS 5007, Villeurbanne, France
[4]Catalyse, Polymérisation, Procédés et Matériaux, CP2M, UMR CNRS 5128, Bât CPE-Lyon, Lyon, France
Email: *ouroagorofaouzou@gmail.com

How to cite this paper: Ouro-Agoro, F., Tchakala, I., Fiaty, K., Charcosset, C., Vanoye, L., Dougna, A.A., Alfa-Sika Mande, S.-L. and Bawa, L.M (2025) Synthesis of a Modified Biosorbent from Lignocellulosic Biomass: Comparative Adsorption Performance with an Activated Carbon of the Same Origin. *Journal of Materials Science and Chemical Engineering*, **13**, 62-84.
https://doi.org/10.4236/msce.2025.1310004

Received: August 26, 2025
Accepted: October 28, 2025
Published: October 31, 2025

Abstract

Mango seed shells were used as a precursor for the synthesis of two adsorbent materials: an activated carbon (AC-MSS) and a modified biosorbent (MB-MSS). The AC preparation process was optimised by evaluating the specific surface area under various activation parameters, while the selection of the most effective MB-MSS was based on its paracetamol removal efficiency. Optimal conditions for AC-MSS synthesis were identified as activation with 40% phosphoric acid, an impregnation ratio of 1.5 (mass of chemical agent/mass of precursor), and carbonisation at 450˚C for 90 min. For MB-MSS, the sample prepared with a sulphuric acid impregnation ratio of 2.5 exhibited the highest adsorption capacity. Both materials were characterised using X-ray diffraction (XRD), Fourier-transform infrared spectroscopy (FTIR), scanning electron microscopy with energy-dispersive X-ray spectroscopy (SEM/EDX), and thermogravimetric analysis (TGA). Kinetic studies revealed that paracetamol adsorption onto both materials followed a pseudo-second-order model. Additionally,

equilibrium data for both adsorbents fitted well to both Langmuir and Freundlich isotherm models. According to the Langmuir model, the maximum adsorption capacities were 44.84 mg/g for AC-MSS and 9.82 mg/g for MB-MSS.

Keywords

Mango Seed Shells, Activated Carbon, Modified Biosorbent, Adsorption, Paracetamol

1. Introduction

Activated carbon (AC) is one of the most widely used adsorbent materials in industrial applications due to its highly developed internal porosity, the diversity of its adsorption sites, and its ability to efficiently retain a broad spectrum of pollutants. Its regenerability and reusability further enhance its appeal in wastewater treatment processes. AC is commonly employed across several sectors, including the food and beverage industry, pharmaceuticals, chemicals, petroleum, mining, nuclear energy, and automotive manufacturing [1]-[3].

Among emerging environmental pollutants, pharmaceutical compounds have become a growing concern. These substances are molecularly diverse, exhibiting various chemical functionalities, a wide range of molecular weights, and complex environmental behaviours. Their high-water solubility and ability to cross biological membranes facilitate their widespread dispersion in aquatic environments. Paracetamol, whose active ingredient is acetaminophen (N-acetyl-para-aminophenol), and is one of the most extensively used drugs due to its analgesic and antipyretic properties [4] [5]. It is classified as a micropollutant or emerging contaminant, alongside personal care products, pesticides, and steroid hormones.

Paracetamol residues are frequently detected in wastewater and surface water, indicating their persistence and potential ecotoxicological effects [6] [7]. Although typically found at trace concentrations (usually below 10 ppm), paracetamol can elicit significant biological responses. In *Daphnia magna*, exposure increases catalase and glutathione S-transferase (GST) activity, suggesting an oxidative stress response, while *Daphnia longispina* shows altered enzymatic activity [8] [9]. In the clam *Ruditapes philippinarum*, exposure modifies oxidative stress biomarkers such as superoxide dismutase and glutathione ratios, revealing significant biochemical disruptions even at low concentrations [10].

Activated carbon has proven effective in removing various pharmaceutical compounds, including paracetamol [11] [12]. However, its high production cost limits its widespread application, particularly in developing countries.

In this context, the present study aims to compare the adsorption efficiency of a modified biosorbent prepared via a simple, low-cost, and locally applicable method with that of activated carbon possessing a high specific surface area. The

ultimate goal is to identify an economically and environmentally sustainable alternative for the treatment of pharmaceutical-contaminated water.

2. Materials and Methods

2.1. Collection and Pre-Treatment of Raw Material

Mango stone shells were used as precursors for the production of a modified biosorbent and activated carbon. To collect the mango stones, a collection system was established by placing a dedicated container within our residential area (in Lomé, Togo), allowing residents to dispose of the stones after consuming the fruit.

The collected stones were thoroughly washed with water to remove surface impurities, then oven-dried (BINDER, Service-Hotline, France) at 105˚C for 24 h. After drying, the kernels were manually separated from the shells. The shells were subsequently ground to reduce their particle size and used as raw material for the synthesis of the adsorbent materials.

2.2. Optimisation and Preparation of Adsorbent Materials

Three parameters were optimised during the preparation of activated carbons: the concentration of phosphoric acid, the impregnation ratio (mass ratio of acid to precursor), and the carbonisation temperature. The aim of this optimisation was to obtain activated carbon with a well-developed specific surface area. For each variation of the selected parameters, the specific surface area of the samples was measured using the BET method. The sample exhibiting the highest specific surface area was considered to correspond to the optimal condition.

In contrast, for the modified biosorbent, only the impregnation ratio was optimised. The various prepared samples were brought into contact with a solution containing the target pollutant for a sufficient period to reach adsorption equilibrium. The sample that adsorbed the greatest amount of pollutant was identified as the one corresponding to the optimal condition.

Activated carbon preparation was presented in a previous paper [13]. For the preparation of the modified biosorbent, the pretreated material was impregnated with concentrated sulfuric acid, using impregnation ratios ranging from 1 to 3. The resulting material was then washed with distilled water until the eluate reached a stable pH.

2.3. Physicochemical Characterisation

Thermogravimetric analysis (TGA) was carried out using a NETZSCH thermobalance (model TG 209 F1). The measurements were performed in porcelain crucibles over a temperature range from ambient to 900˚C, with a heating rate of 10˚C/min under a nitrogen atmosphere. This analysis enabled the assessment of the thermal stability of the materials, with the dual objective of determining, firstly, the optimal conditions for converting biomass into high-quality activated carbon, and secondly, evaluating the impact of chemical and thermal treatments on the thermal properties of the resulting adsorbent materials.

Scanning electron microscopy (SEM, Merlin compact model, Zeiss) was conducted to examine the surface morphology and texture of the samples, with particular attention to the presence of pores and potential surface defects. This analysis was coupled with energy-dispersive X-ray spectroscopy (EDX, Merlin compact model, Zeiss), which provided information on the elemental composition of the material surfaces.

The specific surface area and pore size distribution of the adsorbent were evaluated using a Micromeritics ASAP 2020 analyser, based on the Brunauer- Emmett- Teller (BET) method. Nitrogen was employed as the adsorptive gas, and measurements were conducted at 77 K, the temperature at which nitrogen is in its liquid state. Prior to each analysis, the samples were degassed at 250˚C for approximately 13 h in order to remove any gas molecules previously adsorbed on their surface.

The functional groups present on the surface of the biomass and the synthesised adsorbent materials were identified using Fourier Transform Infrared Spectroscopy (FTIR). The analyses were carried out on powdered samples using an IS50 FT-IR spectrometer, over a wavenumber range of 400 to 4000 cm^{-1}, with a resolution of 4 cm^{-1}.

X-ray diffraction (XRD) is a technique frequently used in materials science to analyse powders, enabling the crystallised mineral phases present in a sample to be identified. Measurements were performed with a powder diffractometer (D8 Advance Bruker) equipped with a copper anode (λ = 0.15418 nm). The samples to be analysed were crushed into a fine powder, scattered in a quartz sample holder and positioned in the diffractometer tower. Each sample was scanned for 2θ from 10˚ to 80˚. All the XRD analyses were conducted at the Henri Longchambon Diffractometry Centre (CDHL) in Lyon, France.

The pH at the point of zero (pH_{PZC}) is a fundamental physicochemical property of materials, defined as the pH at which the surface of the material exhibits no net charge, meaning that the positive and negative surface charges are balanced. The zeta potential of the adsorbent materials was measured using a Malvern Zetasizer Nano ZS analyser (model C) operating at a temperature of 25˚C. For each measurement, 0.1 g of material was suspended in 50 mL of deionised water, previously adjusted to the desired pH using 0.1 N HCl and 0.1 N NaOH solutions. The pH adjustment was performed using a METTLER TOLEDO pH meter. The suspensions were agitated for 1 h at 25˚C to ensure proper homogenisation, then left to stand for 10 min to allow particle settling. Aliquots were subsequently taken from the supernatant for zeta potential analysis. The pH value at which the zeta potential is zero is considered the point of zero charge (pH_{PZC}) of the material.

The determination of water-extractible compounds in the lignocellulosic biomass was carried out according to the method described by Angelini *et al.* [14]. For this purpose, a 4.5 g (w_1) sample of pre-dried biomass powder was mixed with 225 mL of distilled water, corresponding to a solid-to-liquid ratio of 1:50. The mixture was stirred continuously using a magnetic stirrer at room temperature

for 5 h. After extraction, the mixture was filtered using filter paper (w_3), and the solid residue was thoroughly rinsed with distilled water to remove any remaining soluble compounds. The entire filter-residue (w_2) assembly was then dried at 105˚C for 24 h and subsequently weighed. The water-extractable content was calculated using Equation (1):

$$\text{water-extractible}(\%) = \frac{w_1 - (w_2 - w_3)}{w_1} \times 100 \quad (1)$$

The determination of ethanol-extractible compounds in the lignocellulosic biomass was carried out according to the NREL/TP-510-42619 protocol described by Sluiter *et al.* [15]. For this purpose, 2.5 g of dried biomass powder (w_1) previously subjected to water extraction, was placed into a filter paper cartridge (w_3), which was then inserted into a soxhlet extractor. Extraction was performed using 150 mL of 96% ethanol over a period of 10 h, with two extraction cycles per hour. Following the extraction, the cartridge containing the solid residue (w_2) was first air-dried, then oven-dried at 105˚C until a constant weight was reached. The ethanol-extractable content expressed as a mass percentage, was calculated using Equation (2) similar to Equation (1):

$$\text{ethanol-extractible}(\%) = \frac{w_1 - (w_2 - w_3)}{w_1} \times 100 \quad (2)$$

The hemicellulose content was determined using biomass that had been previously dried and deprived of its extractable compounds. For this purpose, a 1.5 g sample was treated with 80 mL of an aqueous sodium hydroxide solution (0.5 M). The alkaline treatment was conducted at 80˚C for 3.5 h to selectively extract the hemicelluloses. Following the treatment, the mixture was filtered, and the resulting solid residue was thoroughly washed with distilled water until a neutral pH was achieved. The residue was then dried at 105˚C for 24 h until a constant weight was reached [16]. The hemicellulose content was calculated using Equation (3):

$$\text{hemicellulose}(\%) = \frac{w_1 - (w_2 - w_3)}{w_1} \times 100 \quad (3)$$

where w_1 represents the mass of the dried, extractive-free biomass sample; w_2 is the combined mass of the biomass residue and the filter paper after alkaline pretreatment and drying; and w_3 corresponds to the mass of the filter paper alone.

The lignin content was determined using biomass that had been previously dried and freed from extractive sulphuric acid (72%) at room temperature under continuous stirring overnight. Subsequently, 135 mL of distilled water were added to the mixture, which was then heated under reflux in a water bath at 100˚C for 2 h. After cooling to room temperature, the solution was neutralised using a 5% sodium bicarbonate solution and filtered. The resulting solid residue was thoroughly rinsed with distiller water and dried at 105˚C for 24 h until a constant weight was achieved [16]. The lignin content was calculated using Equation (4)

$$\text{lignin}(\%) = \frac{w_1 - (w_2 - w_3)}{w_1} \times 100 \quad (4)$$

where w_1 represents the mass of the dried, extractive-free biomass sample; w_2 is the combined mass of the biomass residue and the filter paper after alkaline pretreatment and drying; and w_3 corresponds to the mass of the filter paper alone.

The cellulose content was calculated based on the respective contents of extractives, hemicellulose and lignin, according to Equation (5)

$$\begin{aligned}\text{Cellulose}(\%) = 100 - (&\text{water-extractible} + \text{ethanol-extractible} \\ &+ \text{Hemicellulose} + \text{lignin})\%\end{aligned} \quad (5)$$

2.4. Removal of Paracetamol as the Model Pollutant

The adsorption of paracetamol onto activated carbon (CA-MSS) and the modified biosorbent (MB-MSS) was carried out in batch mode using 250 mL Erlenmeyer flasks containing a total solution volume of 100 mL. The experiments were conducted at controlled temperature (22˚C ± 2˚C) under constant agitation at 200 rpm. The parameter investigated here is the concentration, with the aim of evaluating adsorption kinetics and isotherms. After a sufficient contact time to reach adsorption equilibrium, the different sampled solutions were filtered using a 0.2 µm pore size microfilter. The residual paracetamol concentration was then determined by UV spectrophotometry (METTLER TOLEDO) at a wavelength of 243 nm. The amount of paracetamol adsorbed, denoted as q_{ads} ($mg{\cdot}g^{-1}$), was calculated using Equation (6).

$$q_{ads} = \frac{(C_0 - C_t)V}{m} \quad (6)$$

where C_0 and C_t ($mg{\cdot}L^{-1}$) represent respectively the initial concentration and the concentration at time t in the solution, V (mL) the volume of the solution and m (g) the mass of the adsorbent (activated carbon or biosorbent).

The removal efficiency of paracetamol was determined according to Equation (7):

$$\tau = \frac{C_0 - C_t}{C_0} \times 100 \quad (7)$$

To study the influence of contact time and initial concentration, 0.09 g of activated carbon or 0.18 g of modified biosorbent was brought into contact with 100 mL of a paracetamol solution, with initial concentration ranging from 10 to 30 $mg{\cdot}L^{-1}$, in an Erlenmeyer flask. The mixture was subjected to magnetic stirring at 200 rpm. At regular time intervals, aliquots were withdrawn, filtered through a 0.2 µm microfilter, and subsequently analysed by UV spectrophotometry to determine the residual paracetamol concentration.

To investigate the influence of adsorbent dosage on the efficiency of the adsorption process, various masses of activated carbon (ranging from 10 to 70 mg) or

modified biosorbent (ranging 10 to 100 mg) were brought into contact with a fixed volume (100 mL) of paracetamol solution at a constant initial concentration of 10 $mg{\cdot}L^{-1}$, under the natural pH of the solution. The mixtures were subjected to magnetic stirring under the same experimental conditions as previously described, for a duration exceeding the equilibrium time determined in preliminary experiments. At predetermined intervals, aliquots were withdrawn, filtered using a 0.2 µm microfilter, and subsequently analysed by UV spectrophotometry to determine the residual paracetamol concentration.

For the study of adsorption isotherms (Langmuir and Freundlich), the equilibrium residual concentrations (C_e) and the corresponding adsorbed amounts (q_e) were determined for each adsorbent dosage. These data were subsequently used to plot the adsorption isotherms and to estimate the characteristic parameters of each model from their linearised equations.

The effect of pH on the adsorption efficiency was investigated by contacting 0.09 g of activated carbon or 0.18 g of modified biosorbent with 100 mL of an aqueous paracetamol solution at an initial concentration of 10 $mg{\cdot}L^{-1}$. The experiments were conducted in 250 mL Erlenmeyer flasks at constant room temperature. The pH of the solution was adjusted within the range of 4 to 11 using 0.1 N NaOH or 0.1 N HCl solutions, depending on the desired pH value.

The experiments were performed in triplicate for both kinetic and equilibrium data, and each point on the curves represents the average value of the results obtained from these repetitions.

3. Results and Discussion

3.1. Optimal Conditions of the Prepared Activated Carbon and Modified Biosorbent

Figure 1 illustrates, on the one hand, the effects of carbonisation temperature, phosphoric acid concentration, and impregnation ratio on the BET specific surface area within the context of optimising activated carbon preparation conditions, and on the other hand, the influence of the impregnation ratio with sulphuric acid on the pollutant removal capacity for the preparation of the modified biosorbent.

The evolution of the BET specific surface area as a function of carbonisation temperature (Figure 1(c)) reveals that the maximum value of 1238.9 m^2/g is attained at 450˚C. Furthermore, variation in phosphoric acid concentration (Figure 1(b)) and impregnation ratio (Figure 1(a)) shows no significant improvement in BET surface area below or above the respective value of 40% acid concentration and 1.5 impregnation ratio. These results indicated that the optimal conditions for preparing activated carbon from mango kernel shells correspond to a carbonisation temperature of 450˚C, a phosphoric acid concentration of 40%, and an impregnation ratio of 1.5. Under these conditions, a material exhibiting a well-developed specific surface area is obtained. Conversely, for the preparation of the modified biosorbent, the highest pollutant removal efficiency is achieved at an impregnation ratio of 2.5 (Figure 1(d)).

In previous published work focusing on optimising activated carbon preparation from wood sawdust, slightly different optimal conditions were found: a carbonisation temperature of 500˚C, a phosphoric acid concentration of 40%, and an impregnation ratio of 2, resulting in a BET specific surface area of 1724.7 m^2/g [13]. This difference underscores the decisive influence of biomass type on the development of activated carbon porosity, highlighting the importance of specific optimisation for each lignocellulosic precursor. This observation aligns with the findings of Bhandari *et al.* (2023), who compared different precursors (amla seeds and harro seed) and demonstrated that the optimal conditions for activated carbon production depend on both the precursor type and the activation temperature [17]. Moreover, several recent studies confirm the efficacy of the temperature range employed in this work. Kumar *et al.* reported an optimal temperature of 350˚C for activated carbon derived from banana peels [18]. Purnamawati identified 450˚C as the optimal temperature for sugar palm fronds activated with phosphoric acid [19]. Similarly, Ghibate and al. (2024) utilised 500˚C for thermal activation of *Punica granatum* peels with orthophosphoric acid [20]. Finally, impregnation ratios between 1.5 and 2 are consistent with previous reports; Małgorzata *et al.* [21] employed a WS/H_3PO_4 ratio 1:2, whereas Mohd *et al.* [22] determined that a 1:1 ratio was optimal for coconut shells activated at 700˚C [23].

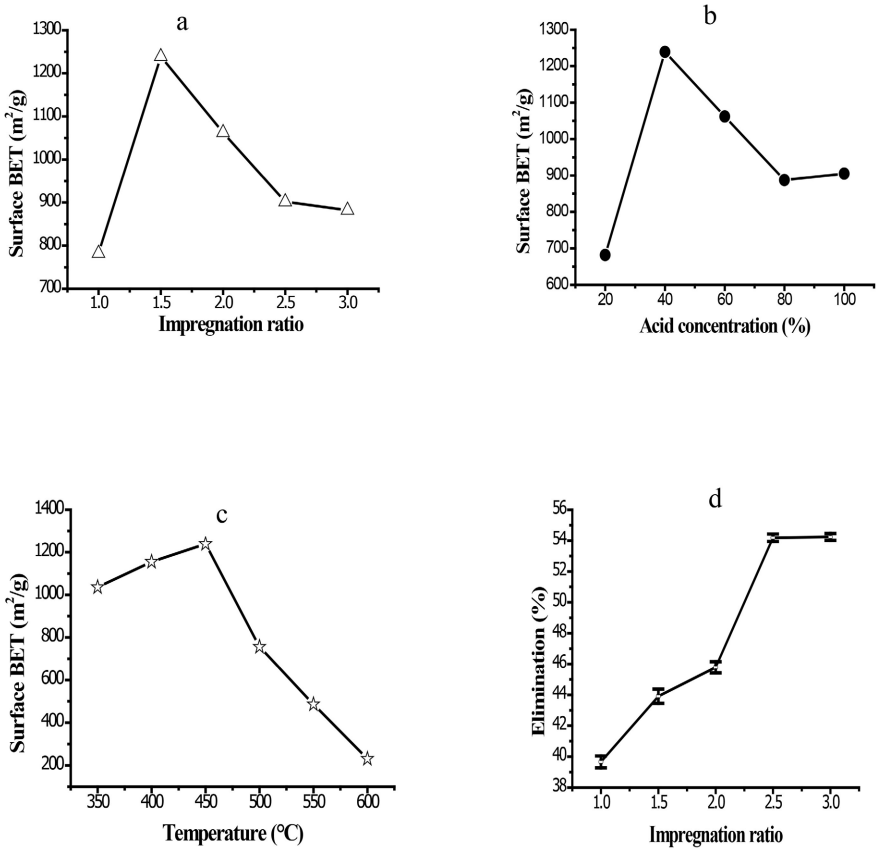

Figure 1. Influence of activation parameters on the BET surface area of activated carbons (a, b and c) and on elimination capacity of the modified biosorbent (d).

The performance of a biosorbent can be influenced by two main parameters: the impregnation ratio and duration. In contrast, temperature has no effect, as the sample is not subjected to a carbonization step. In this study, the impregnation time was not optimized due to the nature and concentration of the activating agent used. Indeed, when plant biomass is exposed to concentrated sulfuric acid, the sample tends to liquefy if left for an extended period. To prevent this phenomenon, the mixture is immediately placed in an oven at 105˚C for 24 hours to ensure proper drying.

3.2. Characterisation of the Precursor and Synthesised Adsorbent Materials

The activated carbon exhibiting the highest BET surface area (1238.9 m^2/g), along with the modified biosorbent, which demonstrated a high removal efficiency, were first characterised and subsequently employed to investigate the adsorption of paracetamol from aqueous solution with the aim of comparing their performance as adsorbent materials.

The thermogravimetric decomposition curves of the raw material (MSS), activated carbon (AC-MSS), and the modified biosorbent (MB-MSS) are presented in **Figure 2**. The TGA/DTG curves obtained for the raw sample (MSS) reveal three distinct decomposition phases: the first phase, spanning 20˚C to 100˚C, exhibits a mass loss of 5.46%, with a thermal peak at 55.8˚C. This stage is attributed to the desorption of water and the release of volatile compounds, associated with the presence of low molecular weight organic substances in the sample [24] [25]. The second phase, from 100˚C to 460˚C, is characterised by a substantial mass loss of the major component of the biomass, notably hemicellulose, cellulose, and partial decomposition of lignin [24] [26]. Finally, the third phase beyond 460˚C shows a lower mass loss of 11.77%, indicating that the material attains thermal stability at this temperature. The decomposition of the main organic constituents appears complete; beyond this threshold, the residual mass consists mainly of ash and minerals, which no longer undergo significant degradation.

Elemental analysis performed using energy-dispersive X-ray spectroscopy (EDX) revealed the presence of elements such as carbon, oxygen, and magnesium in the raw mango seed shells (**Figure 3(a)** and **Figure 3(b)**). The prominent peak associated with carbon indicates a high carbon content, highlighting the suitability of this biomass as a precursor for activated carbon production. Following chemical treatment of the mango seed shells with sulphuric acid (MB-MSS), the EDX spectrum (**Figure 3(c)** and **Figure 3(d)**) showed the disappearance of the magnesium signal. This observation can be attributed to the reaction between magnesium and sulphuric acid, resulting in the formation of magnesium sulphate ($MgSO_4$), a highly soluble salt in acid media. Consequently, this compound is removed during the filtration step, explaining its absence in the solid phase. The EDX spectrum of the activated carbon derived from the treated shells (**Figure 3(e)** and **Figure 3(f)**) further confirms the elimination of mineral elements such as

magnesium, which is explained by their conversion into volatile species or their direct volatilisation at elevated temperatures during pyrolysis, thereby enhancing the purity of the activated carbon. The appearance of phosphorus is ascribed to the terminal decomposition of phosphoric acid, employed as the activating agent, into phosphate species. These phosphate groups may become anchored to the carbon surface, promoting the development of additional active sites. This surface modification significantly improves the pollutant adsorption capacity of the activated carbon by increasing the density of functional sites [27] [28].

The textural characteristics of the activated carbon (AC-MSS) and the modified biosorbent (MB-MSS), both prepared under optimal conditions, are presented in Table 1. Analysis of these data reveals that the activated carbon exhibits a remarkably high specific surface area, whereas the modified biosorbent displays a negligible value, indicating a lack of significant accessible porosity. Furthermore, AC-MSS demonstrates a substantial pore volume (0.71 cm^3/g) and an average pore diameter of approximately 6.05 nm, which is indicative of a predominantly mesoporous structure. These findings are in full agreement with the adsorption-desorption isotherm shown in Figure 4(a), which corresponds to a type IV isotherm according to the IUPAC classification. This type of isotherm, characterised by a distinct hysteresis loop, is typical of mesoporous materials with pore diameters ranging between 2 and 50 nm. The very low BET specific surface area measured for the modified biosorbent (MB - MSS) (0.13 m^2/g) indicates an almost complete absence of pore development, most likely resulting from carbonisation in the presence of concentrated sulphuric acid, which promotes extensive condensation and pore blockage. In this case, the adsorption efficiency of the material is governed not by its porosity but primarily by the abundance of surface functional groups (such as C=O, C-O, and C-N/N-H), which play a decisive role in chemical and electrostatic interactions with paracetamol molecules.

Table 1. Textural characteristics of AC-MSS and MB-MSS.

Adsorbent	BET surface (m^2/g)	Pore volume (cm^3/g)	Pore diameter (nm)
AC-MSS	1238.9	0.71	6.05
MB-MSS	-	-	-

The X-ray diffraction (XRD) pattern of MB-MSS exhibits a single broad peak centred around 23˚, indicative of an amorphous or weakly crystalline structure. This is characteristic of acid-treated materials that have not undergone carbonisation. In contrast, the diffractogram of AC-MSS displays two distinct peaks at approximately 23˚ and 43˚ (Figure 4(b)), suggesting a more ordered arrangement, potentially resulting from partial graphitisation induced by the carbonisation process. In general, biosorbents exhibit a disordered structural organisation, which may limit their adsorption performance. However, they retain a significant capacity to interact with pollutants through mechanisms such as hydrophobic and ionic interactions, making them suitable for specific environmental applications.

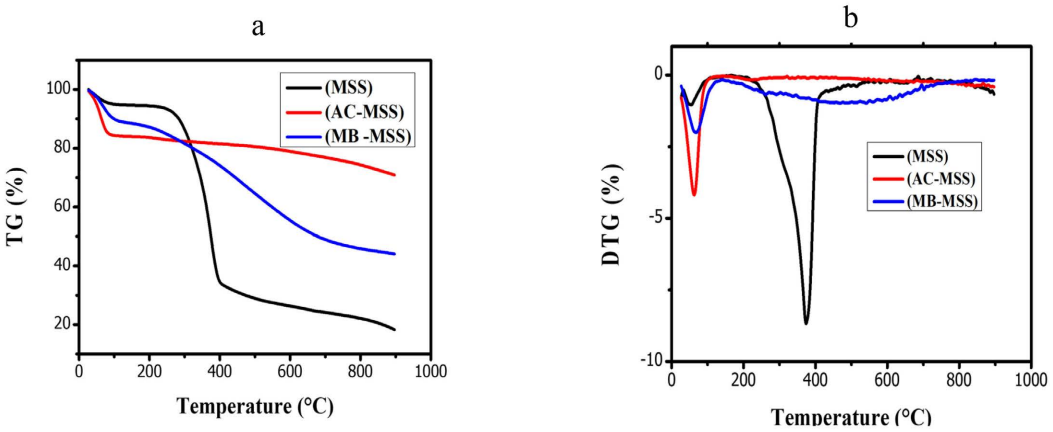

Figure 2. Thermogravimetric curves of MSS, modified biosorbent (MB-MSS) and activated carbon (AC-MSS), (a) TG, (b) DTG.

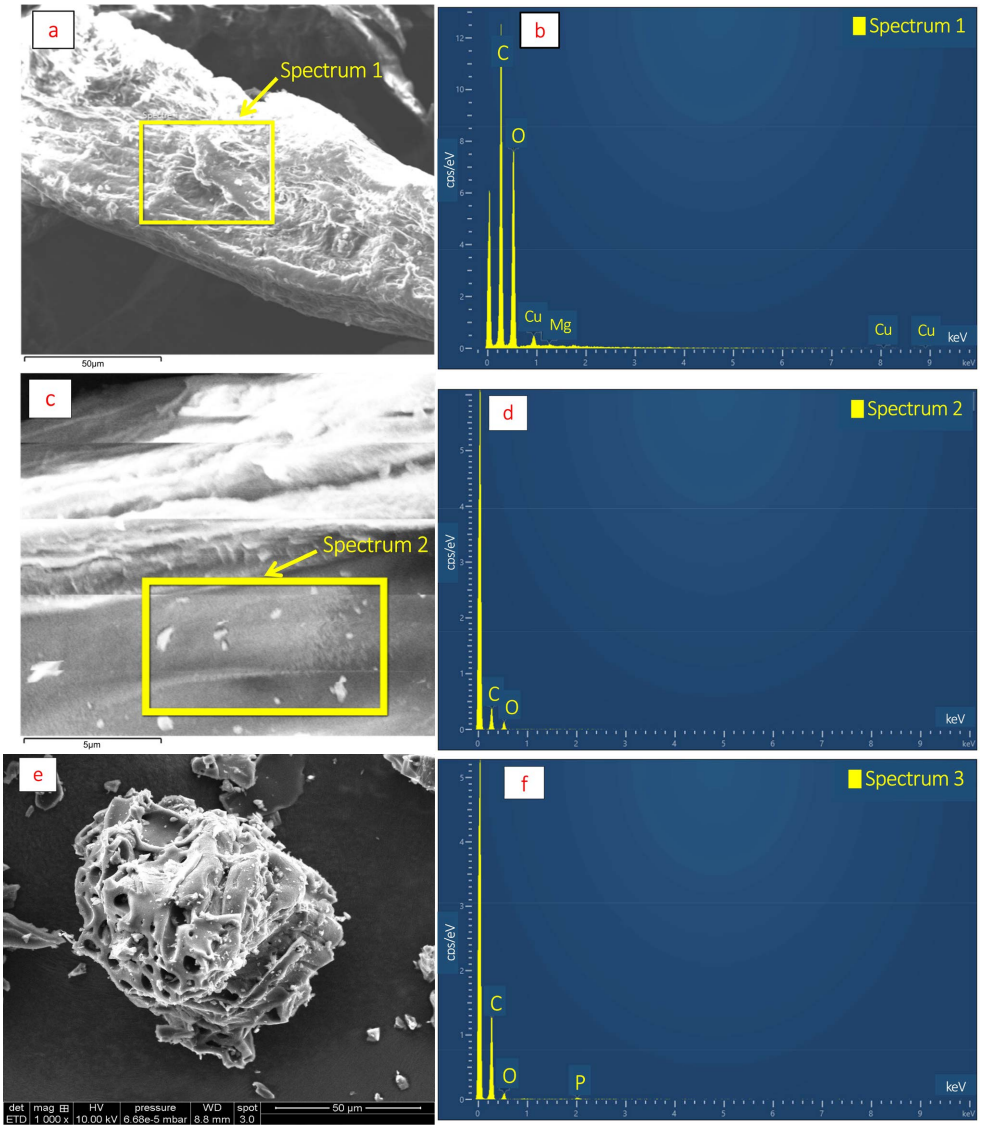

Figure 3. SEM and EDX micrographs of MSS (a, b), MB-MSS (c, d) and AC-MSS (e, f).

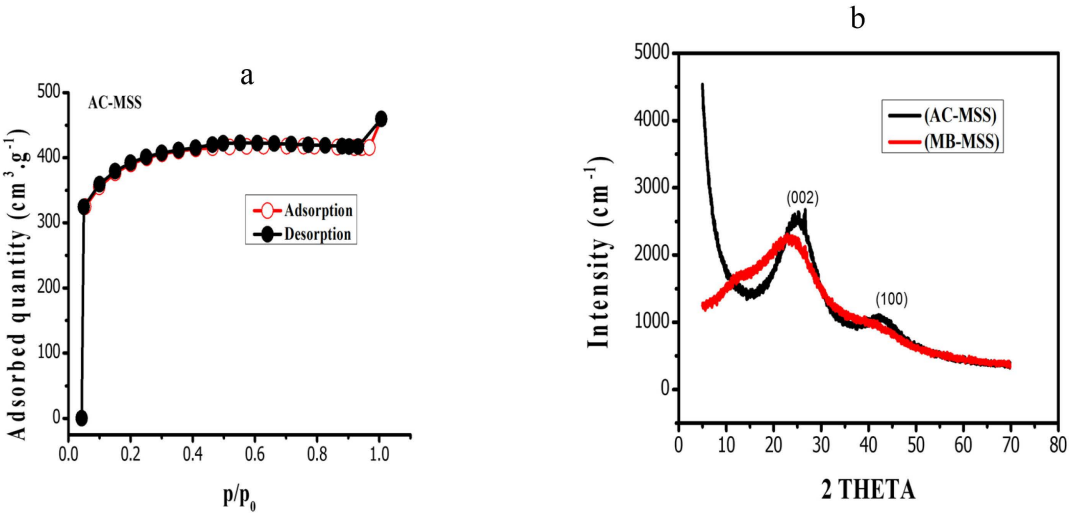

Figure 4. Adsorption-Desorption isotherm of AC-MSS (a) and XRD spectrum of AC-MSS and MB-MSS (b).

The analysis of the infrared (IR) spectra of the adsorbents reveals three predominant absorption bands, whereas the spectrum of raw mango seed shell powder exhibits four main characteristic signals (**Figure 5(a)**).

The FTIR spectrum of the raw mango seed shells shows a broad adsorption band at 3333.4 cm^{-1}, which is associated with the hydroxyl (O-H) stretching vibrations of alcohols and phenolic compounds [29]. The peak at 2916.5 cm^{-1} corresponds to the C-H stretching vibrations present in alcohols, fatty acids, or lipids [30]. The band observed at 1653 cm^{-1} is attributed to the C=O stretching vibrations of esters or carboxylic acids, while the peak at 1030.4 cm^{-1} is assigned to the C-O bending vibrations characteristic of ether linkages [31].

The FTIR spectrum of the acid-treated biosorbent (MB-MSS) exhibits a peak at 1156.3 cm^{-1}, corresponding to C-O stretching vibrations in ethers [29] [31]; a band at 1539.2 cm^{-1}, which is attributed to C-N or N-H vibrations; and a signal at 1652.9 cm^{-1}, ascribed to carbonyl (C=O) group vibrations [29].

In the case of the activated carbon (AC-MSS), the FTIR spectrum shows a speak at 973.7 cm^{-1}, assigned to C-H bending vibrations in aromatic structures [32]; a peak at 1156.6 cm^{-1}, corresponding to C-O stretching in ethers [29]; and a band at 1593.1 cm^{-1}, indicative of C=C stretching vibrations within aromatic rings [33].

The biochemical characterisation of mango stone shell (MSS) biomass reveals a low content of extractable compounds, both in water (7.75% ± 0.15%) and ethanol (3.3% ± 0.06%). This low extractive content indicates a reduced presence of soluble substances such as free sugars, simple phenols, organic acids and waxes, which, if present in significant quantities, could lead to the formation of undesirable by-products during pyrolysis and hinder the development of a well-structured porous network. In parallel, the biomass exhibits a high proportion of structural lignocellulosic polymers, specifically hemicellulose (18.79% ± 1.03%), lignin (39.47% ± 1.80%), and cellulose (30.69% ± 1.30%). These components play an essential role in the formation of cross-linked carbon structures during thermal

treatment. Their controlled decomposition throughout the pyrolytic process contributes directly to the development of porosity and specific surface area-two critical parameters for producing high-performance activated carbon.

Analysis of Figure 5(b) indicates that both activated carbon (AC-MSS) and the modified biosorbent (MB-MSS) exhibit a similar point of zero charge (pH_{pzc}), located around pH 5. This implies that at pH values below 5, the surface of both materials is predominantly positively charged. The surface of the materials is negatively charged at pH values above 5.

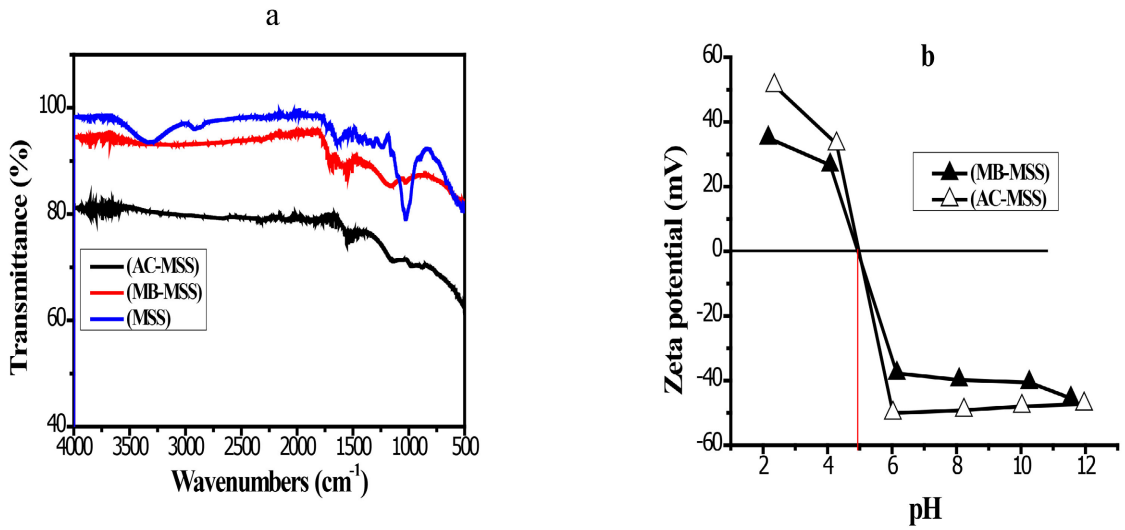

Figure 5. FTIR spectra of MSS, MB-MSS and AC-MSS (a) and determination of pH_{pzc} of MB-MSS and AC-MSS (b).

3.3. Study of Paracetamol Adsorption

In this study, paracetamol is employed as a model pollutant to assess the adsorption efficiency of the synthesised modified biosorbent for the removal of emerging micropollutant from aqueous media. Activated carbon, widely recognised as a benchmark industrial adsorbent [34], is used for comparative purposes to better evaluate the performance of the modified biosorbent. The main physicochemical characteristics of paracetamol are summarised in Table 2.

Figure 6 illustrates the adsorption capacity of paracetamol as a function of contact time at a temperature of 22˚C. The experimental data show that the time required to reach adsorption equilibrium varies depending on the adsorbent used. Activated carbon and the modified biosorbent reach equilibrium after 50 and 90 min, respectively, regardless of the initial paracetamol concentration. At concentration of 10 and 20 $mg{\cdot}mL^{-1}$, the removal efficiency of paracetamol by AC-MSS is very high, exceeding 99%. However, at a higher concentration of 30 $mg{\cdot}mL^{-1}$, a decrease is observed, with a removal efficiency of 92.8%. Similarly, MB-MSS achieves a removal rate of 95.2% at 10 $mg{\cdot}mL^{-1}$, but this efficiency declines with increasing initial concentration. At 20 and 30 $mg{\cdot}mL^{-1}$, the removal rate drops to 62.7% and 48.5%, respectively. The equilibrium adsorption capacities range from 10.9 to 30.8 $mg{\cdot}g^{-1}$ for activated carbon and from 5.2 to 8.1 $mg{\cdot}g^{-1}$ for the modified

biosorbent, depending on the paracetamol concentration.

Table 2. Main physicochemical characteristics of paracetamol.

Molecular formula	$C_8H_9NO_2$
Molecular structure	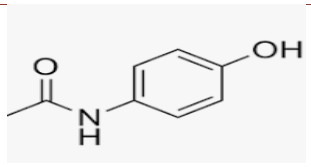
Molecular name	N-(4-hydroxyphenyl) acetamide
Molecular weight	151.17 g/mol
Boiling point	420˚C - 430˚C
Melting point	169˚C - 170˚C
Solubility	Highly soluble in water at 25˚C
Acidity constant	9.5

These results demonstrate that activated carbon exhibits a faster adsorption kinetics compared to the modified biosorbent. This is mainly attributed to its well-developed porous structure and high specific surface area, which enhance both diffusion and accessibility to active sites. Conversely, despite its very low surface area, MB-MSS shows considerable adsorption efficiency at low paracetamol concentrations. However, its limited porosity significantly restricts performance at higher concentrations.

The presence of surface functional groups such as carbonyl (C=O) and amine (N-H) on MB-MSS likely promotes specific interactions with paracetamol molecules. These include hydrogen bonding with the hydroxyl (-OH) and amide (-NH-C=O) groups of paracetamol, as well as dipole-dipole interactions involving the polar group C=O and C-O. These mechanisms contribute to the adsorption process despite the low porosity of the biosorbent.

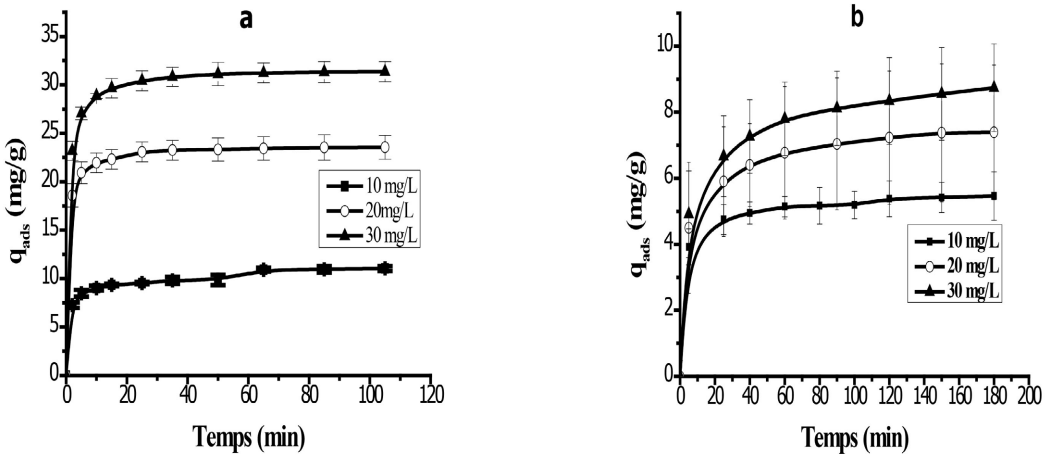

Figure 6. Kinetics of adsorption of paracetamol on AC-MSS (a) and MB-MSS (b) (C_0 = 10 mg·mL^{-1}, V = 100 mL, free pH, $m_{AC\text{-}MSS}$ = 0.09 g, $m_{MB\text{-}MSS}$ = 0.18 g, stirring = 200 rpm).

Figure 7(a) illustrates the effect of the mass of adsorbents derived from mongo seed shells on the percentage removal of paracetamol. Experimental results demonstrate a progressive increase in removal efficiency with increasing adsorbent mass. This trend is consistent, as a greater mass provides a larger number of active sites available for binding paracetamol molecules. For activated carbon, adsorption efficiency increases markedly even at low masses, rising from 43% at 0.01 g to 93.5% at 0.07 g. In contrast, the modified biosorbent exhibits a more gradual increase, reaching a maximum removal percentage of 50.3% at 0.1 g. Furthermore, site saturation does not appear to have been reached within the range of masses investigated for either adsorbent.

Paracetamol contains a phenolic group attached to an aromatic ring, which influences its acid-base behaviour in aqueous solution. It is a weakly acidic compound, with a pKa of approximately 9.5. This value indicates that under acidic to natural conditions (pH < 9.5), paracetamol predominantly exists in its neutral form, with the phenolic hydroxyl group remaining protonated. In contrast, at basic pH values (pH > 9.5), deprotonation of this group occurs, resulting in the formation of an anionic species that is more polar and potentially more reactive in certain environments.

The results regarding the effect of solution pH on paracetamol adsorption by the prepared adsorbents (Figure 7(b)) show that the adsorption efficiency is relatively insensitive to pH variations. This suggests that the dominant adsorption mechanisms are not solely governed by electrostatic interactions, but also involve van der Waals forces and hydrophobic interactions. A slight decrease in adsorption is observed at pH 11, likely due to the deprotonation of paracetamol into its anionic form, which may induce moderate repulsion from the negatively charged adsorbent surfaces ($pH > pH_{pzc}$).

The effect of reactor temperature on the adsorption of paracetamol by the two prepared adsorbents is presented in Figure 7(c) and Figure 7(d). For both adsorbents, a decrease in adsorption capacity is observed with increasing temperature, indicating that the adsorption process is exothermic. This suggests that the heat released during adsorption is sufficient for elevated temperatures to reduce the overall efficiency of the process.

In the context of this study, the pseudo-first-order Equation (8) and pseudo-second-order Equation (9) kinetics models were applied to describe the adsorption mechanism of paracetamol onto the investigated materials. The mathematical expressions corresponding to each of these models are presented below:

$$\ln\left(q_e - q_t\right) = \ln\left(q_e\right) - k_1 t \tag{8}$$

$$\frac{t}{q_t} = \frac{1}{k_2 q_e^2} + \frac{1}{q_e} t \tag{9}$$

q_e and q (mg/g) representing the quantities of triclosan adsorbed respectively at equilibrium and at a time t (min), the kinetic constants of the adsorption reaction are k_1 (min^{-1}) and k_2 ($mg \cdot min^{-1} \cdot g^{-1}$).

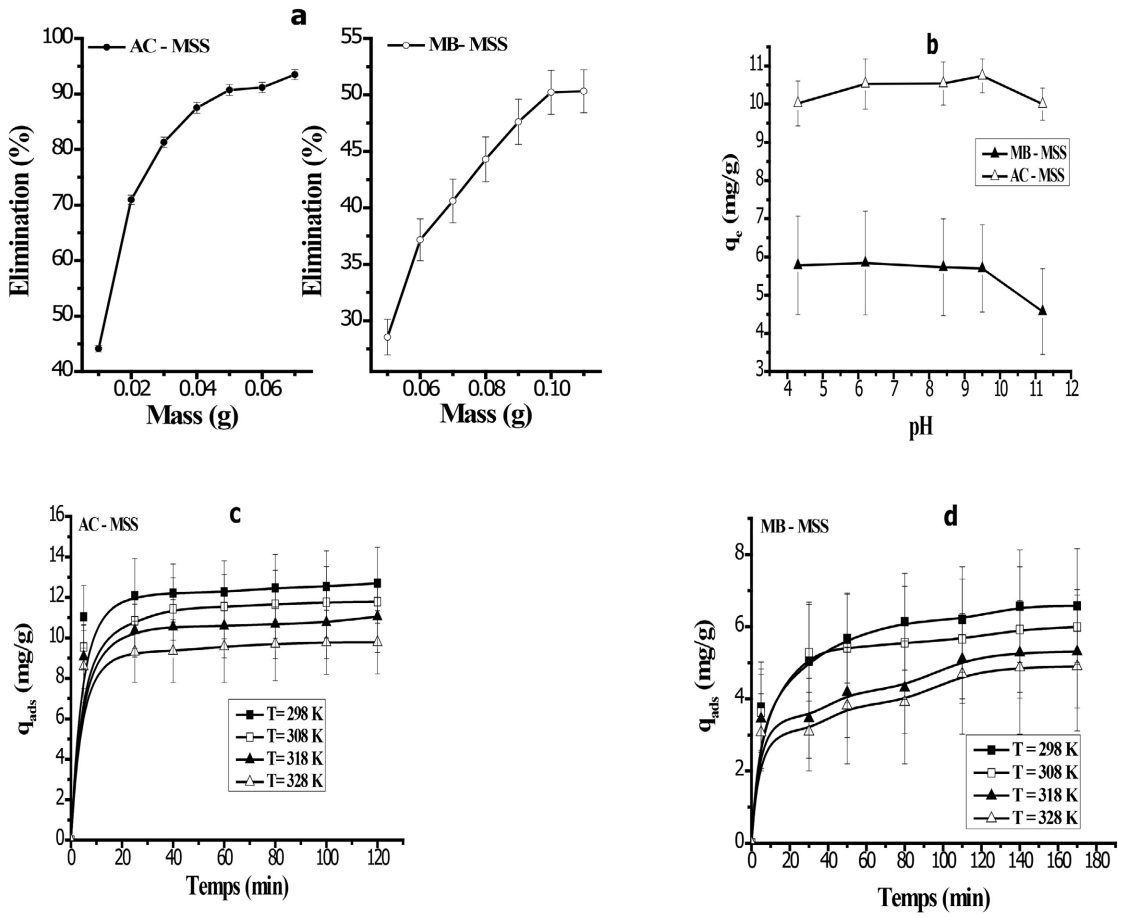

Figure 7. Influence of the mass (a), the solution pH (b) and the temperature (c, d) of adsorbents on the elimination of paracetamol (C_0 = 10 mg/L, V = 100 mL, free pH, $m_{AC\text{-}MSS}$ = 0.09 g, $m_{MB\text{-}MSS}$ = 0.2 g).

The plot of $\ln(q_e - q_t)$ versus time t for activated carbon or modified biosorbent exhibited a linear form (figure not shown). The values of k_1 were calculated from the slope of these lines, and the equilibrium adsorbed quantity $q_{e,cal}$ derived from the y-intercept (in the case of the pseudo-first-order model) and the plot of t/q_t against t for activated carbon or modified biosorbent yielded a linear form (figure not shown). The values of k_2 and $q_{e,cal}$ were determined from the slope and the intercept at the origin of this straight line, respectively (in the case of the pseudo-second-order model).

The kinetic parameters obtained from the pseudo-first-order and pseudo-second-order models are presented in Table 3. Analysis of these results indicates that the experimental data fit the pseudo-second-order kinetic model more accurately, with high correlation coefficients ($R^2 \geq 0.99$) for both adsorbents. Furthermore, the equilibrium adsorption capacities ($q_{e,cal}$), predicted by this model closely match the experimentally observed values ($q_{e,exp}$). These findings suggest that the adsorption mechanism of paracetamol onto both activated carbon (AC-MSS) and the modified biosorbent (MB-MSS) is better described by the pseudo-second-order model, likely involving chemisorption-based interactions.

Table 3. Kinetic parameters of pseudo-first-order and pseudo-second-order kinetic models for paracetamol adsorption onto the activated carbon and modified biosorbent.

	Pseudo-first-order kinetic				
	C_0 (mg/L)	$q_{e,exp}$ (mg/g)	$q_{e,cal}$ (mg/g)	k_1 (min^{-1})	R^2
AC-MSS	10	10.2	2.1	0.014	0.21
MB-MSS	10	5.2	2.8	0.001	0.96
	Pseudo-second-order kinetic				
	C_0 (mg/L)	$q_{e,exp}$ (mg/g)	$q_{e,cal}$ (mg/g)	k_2 ($g \cdot mg^{-1} \cdot min^{-1}$)	R^2
AC-MSS	10	10.2	9.9	0.140	0.99
MB-MSS	10	5.2	7.7	0.063	0.99

In order to assess the maximum adsorption capacities and to elucidate the nature of the adsorption mechanism, the Langmuir and Freundlich isotherm models were applied. The Langmuir model assumes monolayer adsorption onto a homogeneous surface comprising a finite number of identical and energetically equivalent active sites. In contrast, the Freundlich model describes multilayer adsorption occurring on heterogeneous surfaces with non-uniform energy distributions. The linearised forms of these two models are given by Equations (10) and (11), respectively.

$$\frac{1}{q_e} = \frac{1}{q_{\max}} + \frac{1}{q_{\max} K_L} \frac{1}{C_e} \tag{10}$$

$$\ln\left(q_e\right) = \ln\left(K_F\right) + \frac{1}{n} \ln\left(C_e\right) \tag{11}$$

where C_e (mg/L) is the equilibrium concentration in solution, q_e (mg/g) the adsorption capacity of the adsorbate at equilibrium, $q_{\max}$ (mg/g) the Langmuir's constant relating to the maximum adsorption capacity of the adsorbate on a monolayer, K_L (L/mg) represents the Langmuir's equilibrium adsorption constant, K_F ((mg/g) $(L/mg)^{1/n}$) Freundlich constants (that is the adsorption capacity of the adsorbents) and n is the Freundlich isotherm constant related to the adsorption intensity.

The Langmuir and Freundlich isotherm constants, calculated using Equations (10) and (11) as shown in **Figure 8**, are summarised in **Table 4**. All experiments were conducted at a controlled temperature at 22˚C ± 2˚C.

Table 4. Adsorption parameters of Langmuir and Freundlich isotherms for paracetamol.

	Langmuir			Freundlich		
	$q_{\max}$ (mg/g)	R_L (L/mg)	R^2	n	K_F ((mg/g) $(L/mg)^{1/n}$)	R^2
AC-MSS	44.84	0.110	0.98	2.09	7.96	0.99
MB-MSS	9.82	0.039	0.96	2.43	3.69	0.98

Based on the constants derived from the Langmuir and Freundlich isotherms, the AC-MSS material exhibits a significantly higher maximum adsorption capac-

ity (q_{max} = 44.84 mg·g^{-1}) compared to MB-MSS (q_{max} = 9.82 mg·g^{-1}), indicating a greater affinity for the paracetamol. Furthermore, the correlation coefficients (R^2) suggest that the Freundlich model provides a slightly better fit to the experimental data for both materials (R^2 = 0.99 for AC-MSS and 0.98 for MB-MSS), implying that the adsorption process predominantly follows a multilayer mechanism on heterogeneous surfaces. This interpretation is further supported by the values of the Freundlich constant n, which are greater than 1 in both cases (n = 2.09 for AC-MSS and n = 2.43 for MB-MSS), reflecting favourable adsorption. Therefore, AC-MSS demonstrates superior adsorption performance and a more pronounced surface heterogeneity, promoting efficient multilayer adsorption.

The adsorption capacity of paracetamol onto the synthesised adsorbents developed in this study was compared with that of adsorbents recently reported in the literature (see Table 5). Analysis of the data indicates that activated carbon derived from mango seed shells exhibits significant potential as a sustainable and efficient alternative to conventional adsorbents. Although the modified biosorbent obtained from the same precursor material shows a lower adsorption capacity (9.82 mg/g), it remains competitive due to its low cost, widespread availability, and ease of preparation. Furthermore, the relatively mild operating condition (free pH, ambient temperature) provides these materials with an additional environmental and economic advantage.

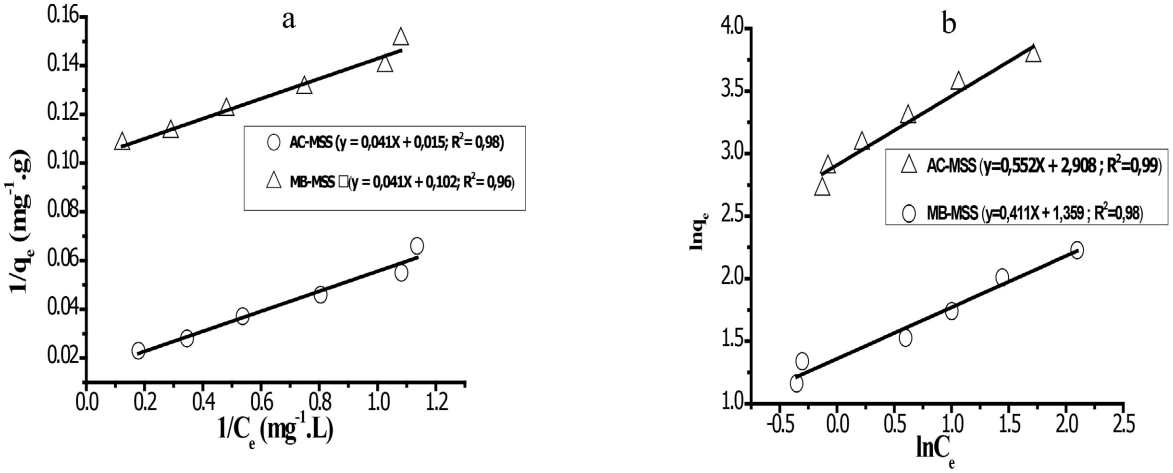

Figure 8. Linearisation of paracetamol adsorption isotherms according to the models: Langmuir isotherm (a) and Freundlich isotherm (b) (C_0 = 10 mg/L; T = 22˚C; V= 100 mL; free pH).

Table 5. Adsorption capacities of paracetamol on various adsorbents from the literature.

Adsorbent	Experimental conditions	Maximum adsorption capacity (mg/g)	Reference
Modified biosorbent from mango seed shell	Batch adsorption C_0= 10 mg/L, free pH, T = 22˚C, m_{AC} = 0.18 g, t_{eq} = 90 min	9.82	this study
Activated carbon from mango seed shell	Batch adsorption C_0 = 10 mg/L, free pH, T = 22˚C, m_{BS} = 0.09 g, t_{eq} = 50 min	44.84	this study

Continued

Activated carbon	Batch adsorption C_0 = 20 mg/L, pH = 7, T = 25˚C, m_{ads} = 0.005 g, t_{eq} = 120 min	31.5	[35]
Activated carbon	Batch adsorption C_0 = 10 - 1000 mg/L, pH = 2, T = 25˚C, m_{ads} = 0.1 g	16.8	[36]
Activated carbon from orange peel	Batch adsorption C_0 = 10 - 100 mg/L, free pH, T = 25˚C, m_{ads} = 0.02 g	49	[37]

4. Conclusions

In this study, three key parameters of the activation process were optimised for the preparation of activated carbon derived from biomass: the carbonisation temperature, the concentration of the chemical activating agent, and the impregnation ratio. The results obtained were compared with those from our previous studies as well as with data reported in the literature using various precursors.

The analysis revealed that carbonisation temperature plays a predominant role in the development of porosity and the enhancement of the specific surface area of the material. Optimisation of this parameter enabled the production of activated carbon with a high specific surface area, thereby improving its effectiveness in the adsorption of paracetamol from aqueous solutions.

The activated carbon produced exhibited a maximum adsorption capacity (q_{max} = 44.84 mg/g), highlighting its potential as a sustainable and efficient alternative to conventional adsorbents. Additionally, a modified biosorbent was also prepared. Although this material showed a lower adsorption capacity (q_{max} = 9.82 mg/g), it remains competitive due to its low cost, abundant availability, simple preparation process, and the use of mild operating conditions (natural pH and ambient temperature), which offer additional environmental and economic advantages.

Thermogravimetric analysis (TGA) and scanning electron microscopy coupled with energy-dispersive X-ray spectroscopy (SEM/EDX) demonstrated that both chemical activation methods for the activated carbon and for the modified biosorbent resulted in materials with good thermal stability. Furthermore, these treatments effectively removed mineral elements originally present in the raw biomass, which could otherwise lead to secondary pollution through leaching if the untreated biomass was directly used in aqueous treatment applications.

Acknowledgements

The authors would like to thank the Cooperation and Cultural Action Service (SCAC) of the French Embassy in Togo for their financial support, Dr. Yves CHEVALIER from the Laboratory of Automation, Process Engineering, and Pharmaceutical Engineering (LAGEPP) for his valuable advice on SEM and his constant availability, Professor Pascal FONGARLAND from the Catalysis, Polymerization,

Process, and Materials Laboratory (CP2M) for welcoming us in his team, and all the administrative and technical staff of LAGEPP.

Conflicts of Interest

The authors declare no conflicts of interest regarding the publication of this paper.

References

[1] Somparn, W., Panyoyai, N., Khamdaeng, T., Tippayawong, N., Tantikul, S. and Wongsiriamnuay, T. (2020) Effect of Process Conditions on Properties of Biochar from Agricultural Residues. *IOP Conference Series*: *Earth and Environmental Science*, **463**, Article ID: 012005. https://doi.org/10.1088/1755-1315/463/1/012005

[2] Halbus, A., Athab, Z. and Hussein, F. (2021) Review on Preparation and Characterization of Activated Carbon from Low Cost Waste Materials. *Egyptian Journal of Chemistry*, **8**, 63-68. https://doi.org/10.21608/ejchem.2021.79055.3870

[3] Yim, Y. and Kim, B. (2023) Preparation and Characterization of Activated Carbon/polymer Composites: A Review. *Polymers*, **15**, Article 3472. https://doi.org/10.3390/polym15163472

[4] Perera, G.W.C.S., de Costa, M.D.P. and Mahanama, K.R.R. (2019) Development of a Fluorimetric Method for Assessing Paracetamol in Pharmaceuticals Tablets. *Journal of Photochemistry and Photobiology A*: *Chemistry*, **368**, 248-253. https://doi.org/10.1016/j.jphotochem.2018.09.039

[5] Aljeboree, A.M. and Alkaim, A.F. (2019) Removal of Antibiotic Tetracycline (TCs) from Aqueous Solutions by Using Titanium Dioxide (TiO_2) Nanoparticles as an Alternative Material. *Journal of Physics*: *Conference Series*, **1294**, Article ID: 052059. https://doi.org/10.1088/1742-6596/1294/5/052059

[6] Kalyva, M. (2017) Fate of Pharmaceuticals in the Environment: A Review. *Theoretical Geoecology in Earth Sciences*, **29**, urn:nbn:se:umu:diva-132995.

[7] Gworek, B., Kijeńska, M., Zaborowska, M., Wrzosek, J., Tokarz, L. and Chmielewski, J. (2020) Occurrence of Pharmaceuticals in Aquatic Environment—A Review. *Desalination and Water Treatment*, **184**, 375-387. https://doi.org/10.5004/dwt.2020.25325

[8] Sousa, A.P. and Nunes, B. (2021) Dangerous Connections: Biochemical and Behavioral Traits in *Daphnia Magna* and *Daphnia Longispina* Exposed to Ecologically Relevant Amounts of Paracetamol. *Environmental Science and Pollution Research*, **28**, 38792-38808. https://doi.org/10.1007/s11356-021-13200-5

[9] Bührer, C., Endesfelder, S., Scheuer, T. and Schmitz, T. (2021) Paracetamol (Acetaminophen) and the Developing Brain. *International Journal of Molecular Sciences*, **22**, Article 11156. https://doi.org/10.3390/ijms222011156

[10] Correia, B., Freitas, R., Figueira, E., Soares, A.M.V.M. and Nunes, B. (2016) Oxidative Effects of the Pharmaceutical Drug Paracetamol on the Edible Clam *Ruditapes philippinarum* under Different Salinities. *Comparative Biochemistry and Physiology Part C*: *Toxicology & Pharmacology*, **179**, 116-124. https://doi.org/10.1016/j.cbpc.2015.09.006

[11] Wakejo, W.K., Meshesha, B.T., Kang, J.W. and Demesa, A.G. (2023) Bamboo Sawdust-Derived High Surface Area Activated Carbon for Remarkable Removal of Paracetamol from Aqueous Solution: Sorption Kinetics, Isotherm, Thermodynamics, and Regeneration Studies. *Water Practice & Technology*, **18**, 1366-1388. https://doi.org/10.2166/wpt.2023.094

[12] Almageed Ali Mohammed, M.A. and A.I. Hamed, T. (2024) Pharmaceutical Wastewater Treatment Using Activated Carbon in a Fixed-Bed Column. *International Journal of Research and Review*, **11**, 429-436. https://doi.org/10.52403/ijrr.20241140

[13] Faouzou, O.A., Ibrahim, T., Amenuvevegab, D.A., Koffi, F., Catherine, C., Seyf-Laye, A.S.M. and Moctar, B.L. (2025) Comparative Study of the Triclosan Adsorption Efficiency by Activated Carbon and Modified Biosorbent Synthesised from a Common Local Precursor. *International Journal of Engineering Sciences & Research Technology*, **14**, 1-15. https://doi.org/10.29121/ijesrtp.v14.i5.2025.1

[14] Angelini, S., Cerruti, P., Scarinzi, G. and Malinconico, M. (2016) Extraction and Fractionation of a Cellulosic Biomass and Its Use as a Bio-Filler in Poly (3 Hydroxybutyrate). *Cellulose Chemistry and Technology*, **50**, 429-437.

[15] Sluiter, A., Ruiz, R., Scarlata, C. and Sluiter, J.D. (2008) Determination of Extractives in Bio-Mass. Laboratory Analytical Procedure, NREL/TP (2008) 510-42619.

[16] Mansora, A.M., Lima, J.S., Anib, F.N., Hashima, H. and Ho, W.S. (2019) Characteristics of Cellulose, Hemicellulose, and Lignin of MD2 Pineapple Biomass. *Chemical Engineering Transactions*, **72**, 79-84.

[17] Bhandari, S., Rajguru, K.B., Gnawali, C.L. and Pokharel, B.P. (2023) Influence of Precursor Type on Activated Carbon Prepared by Phosphoric Acid-Chemical Activation for Supercapacitor Applications. *Journal of Nepal Physical Society*, **9**, 12-17. https://doi.org/10.3126/jnphyssoc.v9i3.62452

[18] Kumar, K., Tyagi, U., Maity, S.K., Singh, S., Sheoran, N. and Kumar, G. (2024) Sustainable Approach for Developing High-Performance Activated Carbon from Agricultural Wastes: Exploring the Impact of Carbonization Parameters and Activating Agents for Enhanced Physiochemical Properties. https://doi.org/10.21203/rs.3.rs-4807116/v1

[19] Purnamawati, N. (2023) Uji Kualitas Sintesis Karbon Aktif Dari Pelepah Aren Teraktivasi Asam Fosfat. *Journal of Research and Education Chemistry*, **5**, 120-129. https://doi.org/10.25299/jrec.2023.vol5(2).15225

[20] Ghibate, R., Ben Baaziz, M., Chrachmy, M., Kerrou, M., Taouil, R. and Senhaji, O. (2024) Production of New Activated Carbon from Agricultural Waste and Its Use as an Eco-Friendly Solution for Removing Copper Ions from Industrial Effluents. *Ecological Engineering & Environmental Technology*, **25**, 96-106. https://doi.org/10.12912/27197050/191363

[21] Wiśniewska, M., Urban, T., Tokarska, K., Marciniak, P., Giel, A. and Nowicki, P. (2024) Removal of Organic Dyes, Polymers and Surfactants Using Carbonaceous Materials Derived from Walnut Shells. *Materials*, **17**, Article 1987. https://doi.org/10.3390/ma17091987

[22] Iqbaldin, M., *et al.* (2013) Properties of Coconut Shell Activated Carbon. *Journal of Tropical Forest Science*, **25**, 497-503. https://www.jstor.org/stable/23616990

[23] Yaceh, N.L., Olakunle, M.S., Maina, N.S., Paul-Emmanuel, T.A. and Yaceh, N.L. (2025) Optimized Removal of Zinc and Copper from Industrial Oil Mill Wastewater Using Coconut Shell-Based Activated Carbon. *NIPES Journal of Science and Technology Research*, **7**, 189-202. https://doi.org/10.37933/nipes/7.2.2025.12

[24] Anukam, A.I., Mamphweli, S.N., Reddy, P. and Okoh, O.O. (2016) Characterization and the Effect of Lignocellulosic Biomass Value Addition on Gasification Efficiency. *Energy Exploration & Exploitation*, **34**, 865-880. https://doi.org/10.1177/0144598716665010

[25] Muigai, H.H., Bordoloi, U., Hussain, R., Ravi, K., Moholkar, V.S. and Kalita, P. (2020)

A Comparative Study on Synthesis and Characterization of Biochars Derived from Lignocellulosic Biomass for Their Candidacy in Agronomy and Energy Applications. *International Journal of Energy Research*, **45**, 4765-4781. https://doi.org/10.1002/er.6092

[26] Bridgeman, T.G., Jones, J.M., Shield, I. and Williams, P.T. (2008) Torrefaction of Reed Canary Grass, Wheat Straw and Willow to Enhance Solid Fuel Qualities and Combustion Properties. *Fuel*, **87**, 844-856. https://doi.org/10.1016/j.fuel.2007.05.041

[27] Xu, W., Liu, J., Sun, K., Liu, Y., Chen, C., Wang, A., *et al.* (2021) Effect of Activation Temperature on Properties of H3PO4-Activated Carbon. *BioResources*, **16**, 4007-4020. https://doi.org/10.15376/biores.16.2.4007-4020

[28] Xu, X., Weng, Y., Zhuang, J., Pei, H. and Wu, B. (2024) Biochar with Phosphoric Acid Modification. *JTICE*, **161**, 105541. https://doi.org/10.1016/j.jtice.2024.105541

[29] Akter, M., Rahman, F.B.A., Abedin, M.Z. and Kabir, S.M.F. (2021) Adsorption Characteristics of Banana Peel in the Removal of Dyes from Textile Effluent. *Textiles*, **1**, 361-375. https://doi.org/10.3390/textiles1020018

[30] Sivachidambaram, M., Vijaya, J.J., Kennedy, L.J., Jothiramalingam, R., Al-Lohedan, H.A., Munusamy, M.A., *et al.* (2017) Preparation and Characterization of Activated Carbon Derived from the Borassus Flabellifer Flower as an Electrode Material for Supercapacitor Applications. *New Journal of Chemistry*, **41**, 3939-3949. https://doi.org/10.1039/c6nj03867k

[31] Benyoucef, S. and Harrache, D. (2015) Caractérisation de la microstructure de sciure de bois de pin sylvestre "Pinus sylvestris" [Microstructure Characterization of Scots pine "Pinus Sylvestris" Sawdust]. *Journal of Materials and Environmental Science*, **6**, 765-772.

[32] Memon, J.R., Memon, S.Q., Bhanger, M.I., Memon, G.Z., El-Turki, A. and Allen, G.C. (2008) Characterization of Banana Peel by Scanning Electron Microscopy and FT-IR Spectroscopy and Its Use for Cadmium Removal. *Colloids and Surfaces B: Biointerfaces*, **66**, 260-265. https://doi.org/10.1016/j.colsurfb.2008.07.001

[33] Puziy, A.M., Poddubnaya, O.I., Martínez-Alonso, A., Suárez-García, F. and Tascón, J.M.D. (2005) Surface Chemistry of Phosphorus-Containing Carbons of Lignocellulosic Origin. *Carbon*, **43**, 2857-2868. https://doi.org/10.1016/j.carbon.2005.06.014

[34] Omri, A., Benzina, M. and Ammar, N. (2013) Preparation, Modification and Industrial Application of Activated Carbon from Almond Shell. *Journal of Industrial and Engineering Chemistry*, **19**, 2092-2099. https://doi.org/10.1016/j.jiec.2013.03.025

[35] Haro, N.K., Dávila, I.V.J., Nunes, K.G.P., de Franco, M.A.E., Marcilio, N.R. and Féris, L.A. (2021) Kinetic, Equilibrium and Thermodynamic Studies of the Adsorption of Paracetamol in Activated Carbon in Batch Model and Fixed-Bed Column. *Applied Water Science*, **11**, Article No. 38. https://doi.org/10.1007/s13201-020-01346-5

[36] Bernal, V., Erto, A., Giraldo, L. and Moreno-Piraján, J. (2017) Effect of Solution Ph on the Adsorption of Paracetamol on Chemically Modified Activated Carbons. *Molecules*, **22**, Article 1032. https://doi.org/10.3390/molecules22071032

[37] Malesic-Eleftheriadou, N., Liakos, E.V., Evgenidou, E., Kyzas, G.Z., Bikiaris, D.N. and Lambropoulou, D.A. (2022) Low-Cost Agricultural Wastes (Orange Peels) for the Synthesis and Characterization of Activated Carbon Biosorbents in the Removal of Pharmaceuticals in Multi-Component Mixtures from Aqueous Matrices. *Journal of Molecular Liquids*, **368**, Article ID: 120795. https://doi.org/10.1016/j.molliq.2022.120795

Abbreviations

AC-MSS: activated carbon made from Mango Seed Shells.
MB-MSS: modified biosorbent made from Mango Seed Shells.
MSS: Mango Seed Shells.